# The effect of the front contact sheet resistance on solar cell performance

M. W. Denhoff, N. Drolet

*Institute for Microstructural Sciences, National Research Council, Ottawa, Canada K1A 0R6*

**Abstract**

The transparent top contact layer of a solar cell is a distributed resistance that cannot be easily represented mathematically. We have used a finite element model to calculate the current distribution in this transparent layer. The calculation gives the voltage drop along the layer as well as the resulting reduction in the current generated in the active layer of the solar cell. *IV* curves generated by the model are used to investigate various methods of experimentally determining series resistance. It is found that the suns-$V_{oc}$ method is the most accurate. A fit of the finite element model to experimental *IV* data from an organic solar cell is used as an example of obtaining solar cell model parameters.

*Key words:* Solar cell, Finite element, Series resistance

## 1. Introduction

Organic solar cells or organic photovoltaic devices (OPVs) have attracted much interest recently as a technology with a potential for inexpensive, clean conversion of solar energy to electricity [1, 2]. Two main approaches have been explored for the realization of efficient OPVs; i) the donor-acceptor bilayer and ii) the donor-acceptor bulk heterojunction [3–5]. Other approaches are also being pursued such as using small molecular organic materials, low band gap polymers, hybrid polymer-inorganic materials, and polymer-polymer bulk heterojunctions [5–10]. As well as improving efficiency, there is also work on improving stability [11] and on large area processing [6, 12–14]. So far, the highest power conversion efficiency has been obtained with polymer-fullerene heterojunctions ( 5%), but various efforts are still in progress to achieve better performance [15–17]. One aspect that limits the efficiency of OPVs is the resistance of the transparent electrode needed in these devices. Among the transparent electrodes available, indium-tin oxide (ITO) has been widely used for the fabrication of organic solar cells. However, transparent conductors such as ITO have higher resistance than good metals, which leads to a substantial resistance in the cells. Up to now, several strategies have been investigated to lower the resistance of the transparent electrodes in devices, with limited success. These include the use of proper electrode designs, of metallic strips and of alternate materials to ITO [18–25].

The resistance of the contact layer is distributed over the area of the device and cannot be treated as a simple lumped circuit element. It is important to have an accurate model of this distributed resistance, since it affects both the efficiency and the determination of internal parameters of the solar cell. There have been a number of attempts to model the distributed resistance of solar cells. Earlier reports use approximations based on a transmission line model[26, 27]. In particular, this lead to a two diode model to approximate the distributed resistance effects. Perhaps the most complete analytical treatment was by Nielsen[28], who derived a pair of coupled, non-linear differential equations to describe the problem. These equations could only be solved approximately. Recently, the front contact distributed resistance problem was solved using a finite element (FE) model[30]. A finite element (FE) model is presented in this paper which adds to that work by adding an internal series resistance to the active layer. Then the consequences of the distributed resistance to power loss, series resistance determination, and model parameter extraction are discussed.

In section 2 of this paper, a model for conduction in the contact layer along with its solution using a finite element calculation will be described. In section 3, some of features of this solution are explored. In particular it was found that the voltage drop increases roughly as the square of the length of the contact layer. Along with this, the solution shows how the net current generated by the solar cell decreases as the voltage drop rises. Recently published papers[31, 32] attribute the reduced performance of organic solar cells as the area increases to resistive losses in the transparent conducting oxide. Our solution illustrates the second cause of loss which is the shutting down of the active layer due to the voltage drop across the transparent conducting layer. In addition, the effects of adding a series resistance internal to the active layer are calculated.

Related to the problem of calculating the effects of the distributed resistance is the problem of measuring the series resistance experimentally. A number of methods have been discussed in the past[26, 27]. A recent review[33] compares various experimental methods with each other, but does not determine their accuracy theoretically. Another review[34] finds that the various experimental determinations of resistance do

---

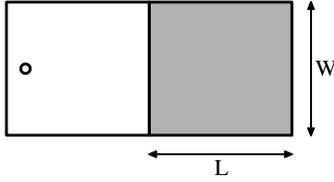*Email address:* `mike.denhoff@nrc.ca` (M. W. Denhoff)

Figure 1: Top view of a solar cell.



Figure 3: Solar cell circuit model. The components inside the dashed box are included in the finite element model.

not agree with each other and they conclude that modeling is needed to clarify the situation. In section 4, a method is given to calculate an effective lumped element resistance which represents the distributed resistance of the contact layer. We then use calculated data to compare three experimental methods of determining series resistance.

Finally, in section 5, our model will be used to analyze measurements of a bulk heterojunction organic solar cell from our lab. This is used as an example to show how the distributed resistance can affect the accuracy of the fit of a theoretical model to measured $IV$ data.

## 2. Model

The geometry considered here is based on simple test devices measured in our lab as sketched in Figure 1. The active area of the solar cell (shaded) is a rectangle with dimensions $L$ and $W$. An indium-tin oxide (ITO) contact layer extends beyond the left edge of the active area to which contact is made for measurements. The resistance of this section of the ITO and of the point contact is simply an external series resistance, $R_{\text{ext}}$.

The solar cell model considered here is a simple three layer structure as shown by the cross-section in Figure 2a). There is an active layer where the illumination generated current, $I_L$, originates. This layer could, for example, be composed of one or more organic layers or of an inorganic semiconductor junction. There is a transparent, conducting contact layer through which light shines into the active layer. Often ITO is used for this contact layer and for simplicity it will be called the ITO layer in this paper. Other materials could be used, in particular, in a semiconductor solar cell it could be a highly doped layer
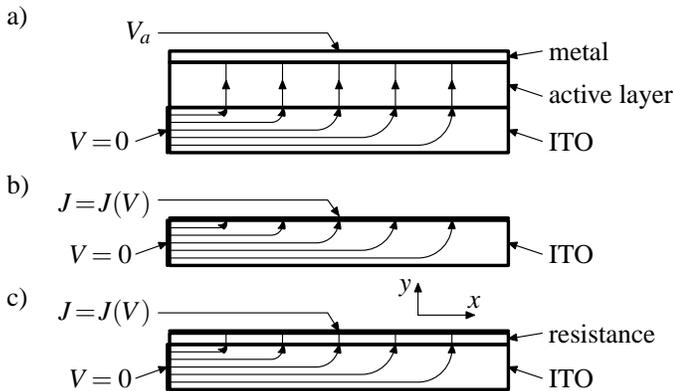


Figure 2: Three solar cell models viewed in cross-section. The orientation of the $x$ and $y$ axes is indicated.
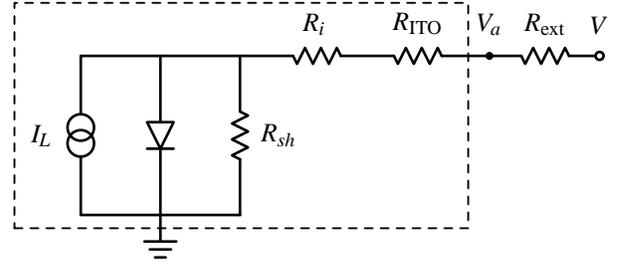
of semiconductor and is often called the emitter layer. There is also a back contact which is a metal with essentially zero resistivity.

Current density, $\boldsymbol{J}$, in a resistive medium can be found using Ohm's law, $\boldsymbol{J} = -\sigma \nabla \phi$. The electrostatic potential, $\phi$, is a solution to the Laplace equation,

$$\sigma_x \frac{\partial^2 \phi}{\partial x^2} + \sigma_y \frac{\partial^2 \phi}{\partial y^2} = 0, \tag{1}$$

where $\sigma_x$ and $\sigma_y$ are the $x$ (horizontal in Fig. 2) and $y$ (vertical in Fig. 2) conductivities. Due to the symmetry of our problem the problem only needs to be solved in two dimensions. The weak form of the above equation is[35]

$$\iint \left( \sigma_x \frac{\partial \phi}{\partial x} \frac{\partial v}{\partial x} + \sigma_y \frac{\partial \phi}{\partial y} \frac{\partial v}{\partial y} \right) dxdy = 0, \tag{2}$$

where $v$ is a weighting function. The model drawn in Fig. 2a) can be solved by imposing the boundary conditions $\phi = 0$ on the left edge of the ITO layer and $\phi = V_a$ on the top boundary of the active layer. If the conductivity of the active layer is much smaller than that of the ITO layer, the current in the active layer will be essentially vertical, as shown in the figure. It is also clear that the current density in the ITO layer is highest at the left edge, near the contact, and drops to zero at the right edge.

The $IV$ response of the active layer is non-linear and it cannot be represented as a simple resistance. Since we are interested in finding the current distribution in the ITO layer, the active layer can be modeled using a current boundary condition in the finite element problem, Fig 2 b), as was done in Ref [30]. The current density must be expressed as a function of the voltage across the active layer, $V_{\text{al}} = (V_a - \phi)$. This is the difference between $V_a$ and the FE solution for $\phi$ along the top edge of the ITO layer (which is a function of $x$). Any model for a solar cell may be used. Following Ref. [30], we will use a simple diode model as an example,

$$J(V_{\text{al}}) = J_0 \left( \exp \left[ \frac{qV_{\text{al}}}{kTn} \right] - 1 \right) + G_{sh} V_{\text{al}} - J_L, \tag{3}$$

where $q$ is the electron charge, $k$ is Boltzmann's constant, $T$ is temperature, $n$ is the diode ideality factor, $J_0$ is the diode saturation current density, $G_{sh}$ is the conductance per unit area and $J_L$ is the current density generated by illumination of the active layer. This diode model may not accurately represent a

bulk heterojunction solar cell [29], but it will serve our purpose of demonstrating the effects of distributed resistance. The above model does *not* include a series resistance, $R_i$, internal to the solar cell. Including $R_i$ in Eq. (3) would lead to a current term inside the exponential. Such an implicit equation for current cannot be applied easily as a boundary condition in the finite element solver.

$R_i$ is not negligible in some types of solar cells based on materials such as organic semiconductors or amorphous or polycrystalline semiconductors like Cu(In,Ga)Se$_2$ (CIGS) and it would be desirable to model the effects of a distributed $R_i$. A series resistance internal to the active layer can be included in the FE model by adding a resistive layer on the top of the ITO as drawn in Fig. 2c). The conductance of this resistance layer, in the $y$ direction, is chosen to model the solar cell internal series resistance. The conductance in the $x$ direction is chosen to be much smaller than the $y$ direction conductance in order to force the current to be vertical in this layer.

The resulting circuit model is drawn in Fig. 3. The lumped elements inside the dashed rectangle are included in the finite element model by the respective distributed quantities. $I_L$, the diode, and $R_{sh}$ are included in the current boundary condition given in Eq. (3). Note that $R_{sh} = (1/A\,G_{sh})$, where $A$ is the area of the active layer and $I_L = J_L/A$. While the lumped resistances $R_{\mathrm{ITO}}$ and $R_i$ are represented by the conductivities of the ITO and resistive layer in the finite element model itself. The resistance, $R_{\mathrm{ext}}$, accounts for external resistances such as in leads and contacts.

Due to the non-linear equation for the current boundary condition, the solution to the problem must be found iteratively. The logic is outlined below.

**Step 1** Guess of initial potential and set applied voltage
$U = U_{\mathrm{guess}}$; $V_a = ?$

**Step 2** Current boundary condition
$J = J(V_a - U)$

**Step 3** Solve FE problem, result $= \phi$

**Step 4** Check for convergence $|\phi - U| < 10^{-7}$
if No go to Step 5; if Yes go to Step 6

**Step 5** Refine potential
$U = U - (U - \phi)/D$; go to Step 2

**Step 6** Calculate total current at contact

$D$ is a number chosen to obtain convergence and was often equal to 2 but sometimes as large as 20. The density of the mesh in the finite element solver was chosen so that the result for the current at the left contact was within 0.3% of the expected answer for $V_a = 0$ of $I = AJ_L$. It was also checked that the calculated current at the left contact was within 0.1% of the current calculated at the top boundary for all values of $V_a$.

The extreme geometry, where the thickness of the ITO is about 100 nm and the length is about 1 cm (i.e. $10^7$ nm), is difficult for the finite element solver to handle. In Ref. [30] this problem was handled by making the ITO layer thicker in the model and then using an appropriately scaled anisotropic conductivity to preserve the current distribution. This technique worked for us. It was tested by comparing the FE solution of a
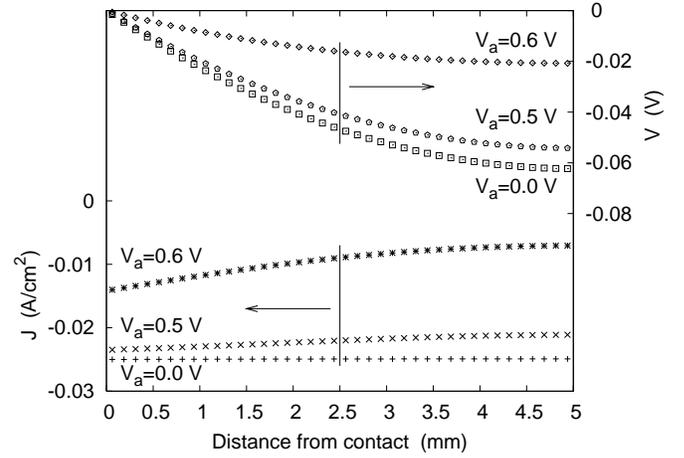


Figure 4: Current density generation in the active layer and voltage distribution in the ITO layer for various applied voltages, for the case of $R_\square = 20\,\Omega_\square$ and internal $R_s = 0$.

4000 nm thick layer with scaled anisotropic conductivity to the solution of a 100 nm thick layer with an isotropic conductivity with a shorter length of $5 \times 10^4$ nm so that both converge in the FE solver. The resulting current distribution was essentially purely in the $x$ direction and uniform across the thickness of the ITO, except very close to the ends of the solar cell. It was also found that simply using a 4000 nm thick model layer with an isotropic conductivity with its value adjusted to give the correct sheet resistance gave the same results.

## 3. Model calculations

In this section, some examples are presented of finite element calculations made using the Freefem++ software (http://www.freefem.org). Calculations were made using the same solar cell parameters as were used in Ref. [30]; $J_0 = 1.9 \times 10^{-6}$ mA/cm$^2$, $n = 1.50$, $G_{sh} = 1.5$ mS/cm$^2$, $J_L = 25$ mA/cm$^2$, and the sheet resistance of the ITO, $R_\square = 20\,\Omega_\square$. This choice was made so that some of the results presented here can be compared with those of Ref. [30]. A specific geometry was chosen of $L = 0.5$ cm and $W = 2$ cm in order to give an area of 1 cm$^2$.

The calculated voltage drop along the ITO layer at various applied voltages, $V_a$, is shown by the top three lines in Fig. 4. As the distance from the contact ($x = 0$) increases, the voltage changes from zero to increasingly larger negative values. The largest values of $V(x)$ occur for a bias of $V_a = 0$, since this is where the current output of the solar cell is maximum, yielding the largest voltage drop along the ITO layer. This voltage drop increases the voltage across the active layer, thus, according to Eq. (3), lowering the net current generated as one moves away from the contact. It shows that regions of a solar cell far from a contact will begin to shut down in conditions of high current and high $R_\square$. The curve for $V_a = 0$ can be derived analytically and is given by $V(x) = R_\square L J_L (x^2/2L - x)$, which agrees exactly with the finite element result.

The net current generation in the active layer is also plotted in Fig. 4. For $V_a = 0$ the current is uniform across the solar
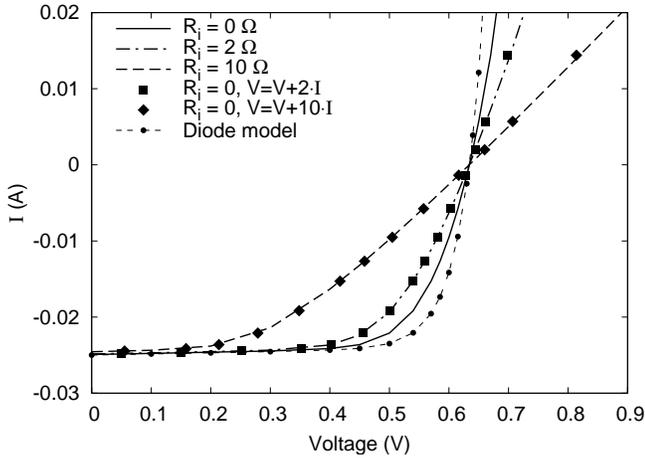
Figure 5: *IV* curves calculated with the finite element model with a ITO sheet resistance of $20\,\Omega_\square$, except the diode model curve which uses $R_\square = 0\,\Omega_\square$.

cell. This is because the current is driven by the photovoltaic current generator in the active layer. As $V_a$ reaches the elbow in the diode curve, the diode begins to turn on and the net current is reduced as a function of distance from the contact. However, at $V_a = 0.5\,\text{V}$ which is near the maximum power point, the current distribution is still fairly uniform. At $V_a = 0.6\,\text{V}$, the current density generated at the end of the active layer far from the contact is about half the value of the current density at the contact end. The non-uniformity grows with higher voltages and while it is not shown, the current distribution is even more non-uniform as $V_a$ is increased above the value of $V_{oc}$.

Calculated *IV* curves are shown in Fig. 5. Comparing the bare diode model (calculated by setting $R_\square = 0$ for the ITO) and the $R_i = 0$ curve shows the effect of the distributed resistance in the ITO layer. The maximum power is reduced from $P_{mp} = 0.5287\,\text{V} \times 0.02258\,\text{A} = 0.01194\,\text{W}$ to $P_{mp} = 0.4970\,\text{V} \times 0.02225\,\text{A} = 0.01106\,\text{W}$ ie. a 7.4 % reduction in power. Comparing these results with those of Ref. [30], there are similar shifts in the *IV* curves and their fill factor changes by up to about 10 %, agrees with our result for power loss.

There is also the question of the source of this power loss. In the literature, it is often assumed that the power reduction of a solar cell with the addition of a series resistance is only due to the $I^2R$ loss [31, 32]. This ignores the loss of current generation due to the resulting forward bias on the active layer. It is difficult to analytically determine the power loss due to a series resistance [36], so it is investigated here with some numerical examples. Using a lumped element model (Eq. (8), with the same parameters as above), for the case that $R_s = 1.6\,\Omega$ the $I^2R$ value is 98.6% of the total power loss. For the case that $R_s = 5\,\Omega$ the $I^2R$ value accounts for 95.0% of the total power loss. For small values of $R_s$ the above assumption that power loss is mainly due to $I^2R$ is fairly good. However, for $R_s = 20\,\Omega$ the $I^2R$ value is only 49.7% of the total power loss. In this case the voltage drop across $R_s$ has biased the diode into its *on* state greatly reducing the generated current.

The FE model can be used to determine the effects of a distributed resistance. In the following section (4.1) the effective

resistance of the ITO layer at the maximum power point is calculated to be $1.608\,\Omega$. The power loss due to this resistance is $I_{mp}^2 R_e = 7.9 \times 10^{-4}\,\text{W}$. This accounts for 90% of the $8.9 \times 10^{-4}\,\text{W}$ power loss found above. That leaves 10% of the power loss being due to the reduction of current generated by the active layer. This can be compared with 1.4% of the power loss being due to reduced $I_{mp}$ found for the $1.6\,\Omega$ lumped resistance above. The reduction of $I_{mp}$ for the distributed resistance $R_e$ is greater than for a similar lumped resistance. As the $I$, $R_\square$, or $L$ increase the shutting down of the active layer, will become larger due to the exponential dependence on the voltage.

Returning to Fig. 5, the $R_i = 2\,\Omega$ and $R_i = 10\,\Omega$ curves show the effects of adding internal series resistance by adding a 10 nm thick resistive layer at the bottom of the active layer in the FE model. For a conductivity of $5 \times 10^{-14}\,[\Omega\text{nm}]^{-1}$ ($1 \times 10^{-14}\,[\Omega\text{nm}]^{-1}$) and assuming a uniform current density across the area of the solar cell, the resistance is $2\,\Omega$ ($10\,\Omega$) for a device with an area of $1\,\text{cm}^2$. As expected, these *IV* curves are further degraded and have lower maximum power points. It is not easily seen in Fig. 5, but larger values of $R_i$ reduce the value of $I_{sc}$. In fact, $I_{sc}$ gets smaller as $R_{sh}$ gets smaller or $R_i$ gets larger.

Another question is whether the internal series resistance can be treated as a simple lumped element resistor. This is tested by starting with the finite element solution for $R_i = 0$ and adding the resistance as a lumped circuit element. That is to modify the voltage by $V \rightarrow V + R_s I$, for the $2\,\Omega$ and $10\,\Omega$ cases, respectively. The agreement below $V_{oc}$ is good, on the scale plotted in Fig. 5, showing that $R_i$ can be well approximated as a lumped element. Above $V_{oc}$ the points of the lumped element calculation are above the line of the full distributed calculation so the internal series resistance cannot be treated as a lumped element here. This shows that using the slope of the *IV* curve at large $V$ as a measure of $R_s$ will be incorrect. The determination of the series resistance will be discussed further in the next section.

## 4. Series resistance determination

The series resistance can be defined operationally as the equivalent resistance at the maximum power point, $R_{eq} = V_{mp}/I_{mp}$. This includes the contribution from every component of the solar cell, the diode, $R_{sh}$, $R_i$, and $R_{ITO}$. This value is important in the design to efficiently couple power to an external circuit. However, in order to help in the design of solar cells and to help understand internal physics it is useful to be able to separate out the contribution to $R_{eq}$ due to the series resistance. Here "series resistance" refers to the combination of $R_i$, $R_{ITO}$, and $R_{ext}$.

A number of methods to obtain the series resistance experimentally have been reviewed by Ref. [33]. The various methods were compared with each other, but not against an expected "theoretical" value. The best two of these methods will be used to determine the series resistance with calculated data. First the theoretical value must be found.

### 4.1. Calculation of series resistance

Consider the contribution of the ITO layer to the series resistance. Since the total current does not flow through the entire ITO layer, an effective resistance, $R_e$, must be used. It can be defined using the definition of power, $P = I^2 R_e$. The actual power dissipated in the ITO layer can be found by integrating the following expression,

$$P = \iiint J^2 \rho \, \mathrm{d}x\mathrm{d}y\mathrm{d}z, \qquad (4)$$

where $J$ is the current density and $\rho$ is the resistivity of the ITO layer. Since the current is uniform across the cross-section of the ITO, this can be written,

$$P = \frac{\rho}{A_{\mathrm{ITO}}} \int J^2 \mathrm{d}x, \qquad (5)$$

where $A_{\mathrm{ITO}}$ is the area of the cross-section of the ITO layer. The effective series resistance is found using the power and the total current,

$$R_e = \frac{P}{I_t^2}. \qquad (6)$$

When $V_a = 0$, the current in the ITO (in the $x$-direction) is $I(x) = (I_t/L)x - I_t$. It is straight forward to find that

$$R_e = \frac{R_\square L}{3W} = 1.667 \, \Omega, \quad \text{for } V_a = 0, \qquad (7)$$

for the above example solar cell. This is the same result as that derived by Nielsen [28].

Using the finite element calculation for the above solar cell, and doing a numerical integration gives the effective resistance for the short circuit condition to be $R_e = 1.657 \, \Omega$. The small difference between this and the exact result above, could be due to numerical error or due to the assumption that the current is uniform in the ITO layer not being correct very near either end of the solar cell.

At other operating voltages the current distribution will change, which should change the effective resistance. At the maximum power point, the finite element calculation gives; $V = 0.5 \, \mathrm{V}$, $R_e = 1.608 \, \Omega$, and just below the open circuit voltage; $V = 0.6 \, \mathrm{V}$, $R_e = 1.346 \, \Omega$. The change from short circuit to maximum power point is small (16%), but at higher $V_a$ the change is larger and it is no longer a good approximation to treat $R_s$ as a constant. Finally, the total series resistance is given by the sum $R_s = R_i + R_e + R_{\mathrm{ext}}$.

### 4.2. Fitting diode model to IV curve

One method of determining $R_s$ (and other parameters) involves fitting the full diode circuit model to the measured IV curve. This is somewhat complex, so the method of fitting will be discussed here. The diode circuit model is given by

$$I(V) = I_0 \left( \exp \left[ \frac{q(V - IR_s)}{kTn} \right] - 1 \right) + \frac{V - IR_s}{R_{sh}} - I_L, \qquad (8)$$

where the diode saturation current is $I_0 = J_0/A$ and the other symbols have been defined previously. Unfortunately, this is
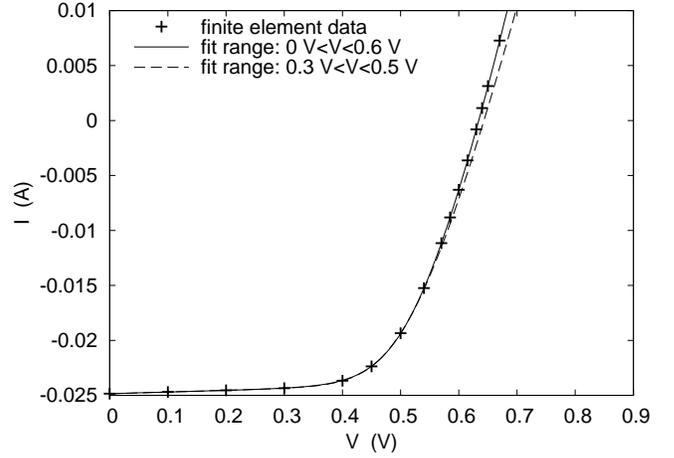
Figure 6: Calculated IV data along with fits to the diode circuit model with different ranges for the fit.

an implicit function for $I(V)$, which makes it difficult to use automatic fitting programs.

The shunt resistance, $R_{sh}$, can be determined by simply finding the slope of the IV curve at $V = 0$. This can be seen mathematically by calculating the total derivative of Eq. (8) with respect to $V$. This was also checked with generated data from the finite element model.

The remaining parameters, $n, I_0, R_s$, all have strong effects on the rising part of the IV curve, making fitting by hand using trial and error quite tedious. It has been shown [37] that the semiconductor diode curve can be expressed as a function of $V$ using the Lambert $W$ function. A description of the Lambert $W$ function is given in Ref. [38]. For $R_s/R_{sh} \ll 1$, the current can be expressed using the Lambert $W$ function (see Appendix A),

$$I_W = \frac{nkT}{qR_s} W\left( \frac{qR_s I_0}{nkT} \exp\left[ \frac{q}{nkT}\left(V - \frac{VR_s}{R_{sh}} + I_L R_s + I_0 R_s\right) \right] \right)$$
$$+ \frac{V}{R_{sh}} - I_L - I_0, \qquad (9)$$

where $W$ is the solution to $x = W(x)\mathrm{e}^{W(x)}$. Due to the approximation, $I_W$ has a slight inaccuracy near $V = 0$ where $I$ is large for a solar cell. This can be corrected, with good accuracy, by replacing $I_L$ in the equation with $I_{sc}$.

Eq. (9) can be fit to data calculated using the FE model, using $R_i = 2 \, \Omega$, $n = 1.5$, $I_0 = 1.9 \times 10^{-9}$, and $R_\square = 20 \, \Omega_\square$. The series resistance, $R_s$, will be the sum of the internal $R_i$ and the effective resistance, $R_e$, of the ITO layer. The value of $R_e$ varies with $V_a$ and was calculated using the same method as in the previous section. Theoretically, (ie, from the model) at $V_{\mathrm{mp}} = 0.46 \, \mathrm{V}$, $R_e = 1.61 \, \Omega$ which gives $R_s = 3.61 \, \Omega$ and at $V_a = 0.6 \, \mathrm{V}$, $R_e = 1.43 \, \Omega$ which gives $R_s = 3.43 \, \Omega$.

Fits were performed with a non-linear least-squares method, using the Marquardt-Levenberg algorithm (using the program gnuplot; http://www.gnuplot.info). The solid line in Fig. 6 shows the result of fitting Eq. (9) to data calculated using the FE model over the voltage range $0 \, \mathrm{V} \leq V \leq 0.64 \, \mathrm{V}$, which gives $R_s = 3.44 \, \Omega$, $n = 1.61$, and $I_0 = 6.00 \times 10^{-9} \, \mathrm{A}$ as the fitting parameters. The fit results for $n$ and $I_0$ are significantly
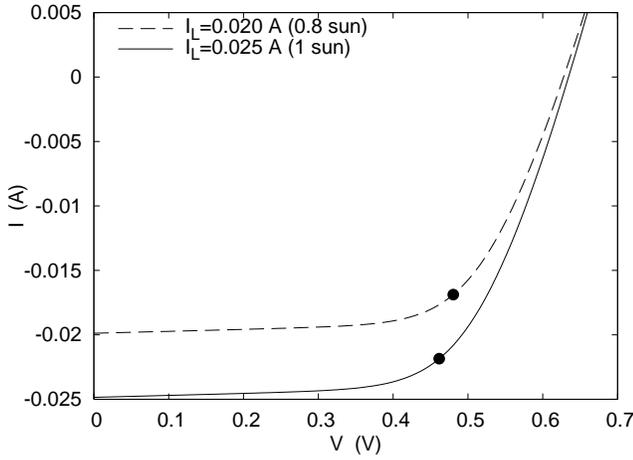
Figure 7: Calculated *IV* curves at two illumination intensities. The dots mark the points with a current shift, $\Delta I = 0.003$ A.
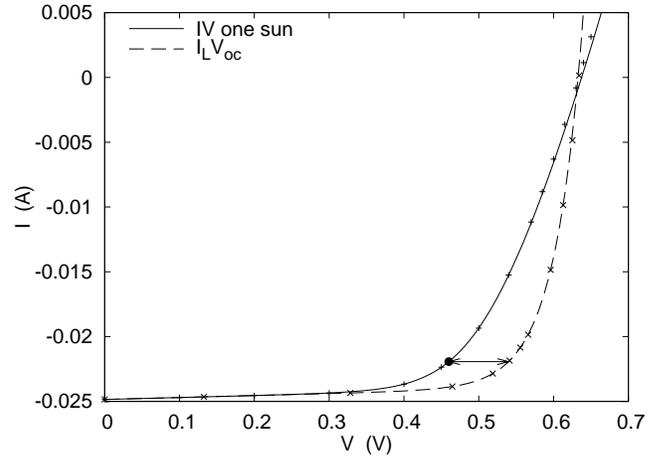


Figure 8: Plot of calculated $I_L$ vs $V_{oc}$ along with a one sun *IV* curve. The maximum power point is marked with a dot. The voltage shift is indicated by a double arrow.

different than the values which were used in the FE model to calculate the points. This error in reproducing the model parameters is similar to the findings in Ref. [30]. The value of $R_s$ from the fit is close to the theoretical value for $V_a = 0.6$ V, but it is somewhat lower than the theoretical value at $V_{mp}$.

On the other hand, if the fit is done over the range $0.3$ V $\leq V \leq 0.5$ V, the fitting values are $R_s = 4.15\,\Omega$, $n = 1.50$, and $I_0 = 1.57 \times 10^{-9}$ A. Evidently, if the fit is performed at the bend of the *IV* curve, more accurate values of $n$ and $I_0$ are obtained. The fit value of $R_s$ is somewhat higher than the theoretical value at $V_{mp}$ of $R_{s,mp} = 3.61\,\Omega$. This fit, shown by the dashed line in Fig. 6, departs visibly from the data at high values of $V$.

The values of fitting parameters are very sensitive to the fitting method. The reason for this is that Eq. (9) does not include the effects of the distributed resistance. The case of experimental data with errors is more complex. If the size of the errors is larger than about the thickness line in Fig. 6 (about $\pm 0.0001$ A), it would be difficult distinguish between the above two fits in the range $0.3$ V $\leq V \leq 0.5$ V. This would create a greater uncertainty in the value of $R_s$.

### 4.3. Two IV curves at different illuminations

One of the two best methods of determining $R_s$ as judged in Ref [33], is to measure two or more *IV* curves with different illumination levels. Points are marked on each curve at a fixed current, $\Delta I$, up from $I_{sc}$. The slope of the line joining these gives the inverse of $R_s$. Calculated data, with the same solar cell parameters as in the previous section, for illumination of 1 sun and 0.8 sun are plotted in Fig. 7. Points are marked on each curve at $\Delta I = 0.003$ A, which was chosen to put the point at $V_{mp} = 0.46$ V on the 1 sun curve. The inverse of the slope of the line defined by these points is

$$R_s = \frac{\Delta V}{\Delta I_{sc}} = 3.74\,\Omega.$$

This is close to but slightly higher than the theoretical result of $3.61\,\Omega$.

The resistance was also calculated using $\Delta I = 0.004$ A. This gave $R_s = 3.61\,\Omega$. This is equal to the theoretical value. This method of determining $R_s$ finds a value close to the true value, but it depends on choosing the correct $\Delta I$. The problem is that there is no exact rule for choosing the point other than that it should be slightly above $V_{mp}$. This results, for our example, in a possible error up to $6\%$.

### 4.4. $I_L$-$V_{oc}$ plot

The second of the two recommended methods from Ref. [33] is to use a plot of light intensity or $I_L$ vs $V_{oc}$. Experimentally this means measuring $V_{oc}$ for a range of illumination intensities from zero up to some maximum, typically one sun. If $R_s$ is not too large and $R_{sh}$ is not too small, the measured value of $I_{sc}$ can be used for the value of $I_L$. Since there is no current flowing at $V_{oc}$, this data eliminates the effects of the series resistance. The difference between the $I_L$-$V_{oc}$ curve and the *IV* measured at the chosen maximum illumination is due to $R_s$.

Fig. 8 shows the calculated $I_L$-$V_{oc}$ data using the finite element model and the same parameters as the previous section. As shown in the figure, the voltage difference is found at the current level of the maximum power point of the *IV* curve. From this the series resistance is

$$R_s = \Delta V/I_{mp} = 3.64\,\Omega. \tag{10}$$

This is close to the finite element calculation value of $3.61\,\Omega$. (for $V_a = 0.5$ V.) As expected, this shows that the suns$V_{oc}$ method does not depend on any specific model of the solar cell, in particular, it is not affected by the distributed nature of the resistance of the ITO layer.

## 5. Experimental results

In this section, the measured *IV* data from an organic solar cell is fit to the FE model as an example.
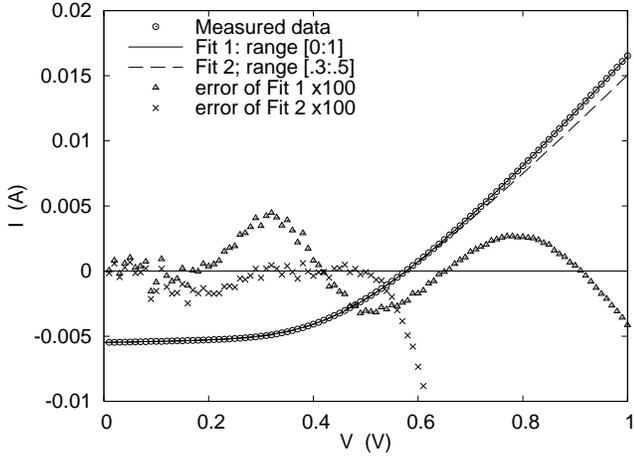
Figure 9: Fits of diode model (Eq. 9) to measured data. The parameters of the two fits are given in the text.



Figure 10: Fit of finite element model to measured *IV* of an actual solar cell. Lines are drawn as a guide to the eye.

## 5.1. Device preparation and measurement

In a glove box, P3HT (Rieke Metals) was first dissolved in 1,2-dichlorobenzene (DCB) at 40 °C for 2 h to make a solution concentration of 17 mg/mL. Then, PCBM (American Dye Source, Inc.) was added in 50 wt% to have a P3HT:PCBM solution ratio of 1:1 wt/wt. The blend was stirred at 40 °C for 14 h. The solar cells were prepared on commercial ITO-coated glass substrates (Applied Films Corp) with a measured sheet resistance of $11 \, \Omega_\square$. Each substrate ($5 \times 5 \, \text{cm}^2$) had been patterned using photolithography technique to produce eight segments with an active device area of $0.55 \times 0.76 \, \text{cm}^2$. Prior to use, the substrates were cleaned sequentially with detergent, deionized water, acetone, ultrasonicated isopropanol at 80 °C, and were treated with UV/ozone plasma for 15 min. A thin layer ( 55 nm) of poly (ethylene dioxythiophene:polystryrene sulfonate) (PEDOT-PSS, Baytron P) was first spin-coated at 5000 rpm for 60 s onto the ITO substrate and then dried at 120 °C for 1 h. Then, the active layer was obtained by spin-coating the P3HT:PCBM (1:1) solution at 600 rpm for 60 s. After spin-coating, the film was slowly dried in a covered glass petri dish for 24 h to form a thin film with a thickness of ≈120 nm. The thickness of spin-coated films was measured with a surface profilometer (DektakIII, Vecco Instruments Inc.). Then, the substrate was transferred to an Edwards multi-source evaporator for subsequent material deposition. In order, LiF (1 nm) and Al (150 nm) were deposited by thermal evaporation at a pressure of $\approx 1 \times 10^{-7}$ Torr and at room temperature.

The solar cells with no protective encapsulation were tested in air under air mass (AM) 1.5 simulated solar illumination (100 mW/cm², Sciencetech Inc., Model SF150). *IV* characteristics were recorded using a computer-controlled Keithley 2400 source meter. *IV* data measured on one device is presented in Fig. 9. In summary the main properties of this device are $I_{sc} = 0.0056$ A, $V_{oc} = 0.576$ V, fill factor = 0.52, and power efficiency = 3.8%.
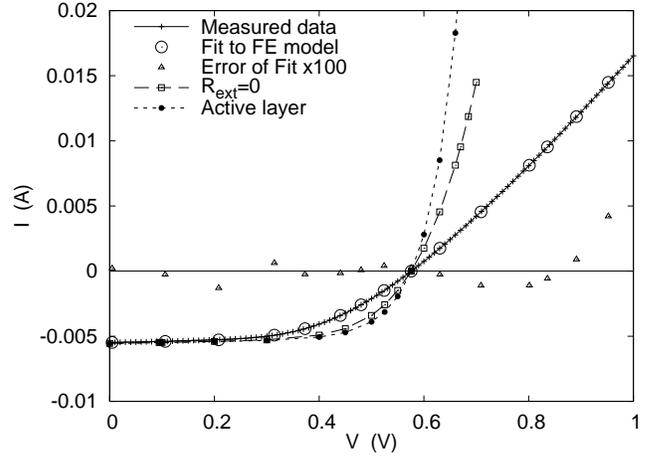
## 5.2. Data fit to discrete diode model

It is common to fit the diode model to experimental data. Our data was fit by first determining $R_{sh} = 1389 \, \Omega$ from the slope near $V = 0$, and then using a non-linear least squares method to fit Eq. (9) to the data. Fig. 9 shows fits to the diode model over different ranges of $V$. Fit 1 was made over the range $0 \leq V \leq 1$ V and yields $n = 2.46$, $I_0 = 5.8 \times 10^{-7}$ A/cm², and $R_s = 20.2 \, \Omega$. Fit 2 was made over the range $0.3 \, \text{V} \leq V \leq 0.5$ V and yields the values $n = 2.15$, $I_0 = 1.6 \times 10^{-7}$ A/cm², and $R_s = 23.0 \, \Omega$. The plotted errors of the fits were found by taking the difference between the values of Eq. (9) and the data and multiplying that by 100. While Fit 1 looks good on the scale of the plotted data, the error plot shows that the fit is not perfect. The fit over a narrower range of voltage, Fit 2, agrees with the data, within the measurement noise, for $0 \leq V \leq 0.5$ V. The dip in the error points near $V = 0.2$ V reflects a similar fluctuation in the data. Above $V = 0.5$ V there is a poor fit. The two fits result in substantially different parameters, so it is important to determine which is better. The FE modeling in the previous sections show that the series resistance can be treated as roughly constant below $V_{oc}$ and it begins to vary significantly above that. This implies that Fit 2 should give more accurate results for the operating parameters of a working solar cell.

## 5.3. Data fit to distributed finite element model

The data can also be fit with the FE model, with the dimensions of the active layer $L = 7.6$ mm and $W = 5.5$ mm. First the sheet resistance of the ITO was measured to be $11.00 \pm 0.05 \, \Omega_\square$. The resistance of the ITO connecting layer not under the active layer (left side of Fig. 1) could not be determined accurately because it depends on the mechanical placement of a point contact in the experimental jig. However, $R_{ext}$ is approximately $20 \, \Omega$. With such a large value of $R_{ext}$ it is not possible to separate out the contribution of a possible internal series resistance of the active layer. This resistance was set to zero in the model. The fit was done by assuming $R_{ext}$ and $n$ values, then using the FE model choose the parameters $J_L$ and $J_0$ that fit the data at $V = 0$

and $V = V_{oc} = 0.5759$ V. A number of points were then calculated to map out the $IV$ curve and the average squared error was calculated. A new value of $n$ was chosen and the above repeated and the two results compared to see which was the better value of $n$. This procedure was iterated manually until the best values of $n$ and $R_{ext}$ were found. A wide range of $n$ and $R_{ext}$ values were tried to ensure that this was not just a local minimum. This method is completely mechanical and, in principle, could be done by a computer program. In the end $n$ could be determined with a precision of about $\pm 0.1$ and $R_{ext}$ within about $\pm 0.3 \, \Omega$.

The best fit of the FE calculation over the whole range of $V$ is plotted in Fig. 10. Values of $J_L$ and $J_0$ that were determined in the above fitting procedure were converted into current by multiplying by the area if the device. The resulting parameters are $n = 2.15$, $I_0 = 1.63 \times 10^{-7}$ A, $I_L = 5.58 \times 10^{-3}$ A, and $R_{ext} = 17.4 \, \Omega$. The error of the fit is shown in the Fig. 10 and the fit is within the experimental noise for $V < 0.8$ V. Above this the organic solar cell is no longer precisely following the FE model, possibly due to $R_i$ not being included. The values of $n$ and $I_0$ are in good agreement with Fit 2 using the Lambert $W$ function.

In order to compare the series resistance fits, the equivalent resistance of the ITO layer under the active layer was computed from the FE model, using the method described in subsection 4.1. The result depends on the operating point of the device and some values are: $R_e(V=0) = 5.04 \, \Omega$, $R_e(V=V_{mp} \approx 0.38 \, V) = 4.90 \, \Omega$, and $R_e(V=0.80 \, V) = 3.38 \, \Omega$. At the maximum power point the total series resistance is $R_s = R_{ext} + R_e = 17.4 + 4.9 = 22.3 \, \Omega$, which is slightly less than the value obtained from Fit 2. On the other hand, at $V = 0.80$ V, $R_s = 20.8 \, \Omega$, which is closer to the value from Fit 1.

In order to see the effect of the ITO, there are two more plots in Fig. 10. One shows the $IV$ curve for $R_{ext} = 0$. There is a significant improvement over the data with the maximum power going from $P_{mp} = 1.6$ mW to $P_{mp} = 2.0$ mW and the fill factor changing from $ff = 0.52$ to $ff = 0.63$ for the measured data and the $R_{ext} = 0$ simulation, respectively. A final plot has, in addition to $R_{ext} = 0$, the sheet resistance of the ITO under the active layer set to zero. This gives an $IV$ plot for the bare active layer. The solar cell characteristics further improve to $P_{mp} = 2.1$ mW and $ff = 0.67$. The distributed resistance of the ITO under the active area reduces the power output by about 5%.

In our experimental geometry, $R_{ext}$ is a large problem in that it degrades the performance of the solar cell and also that makes extracting the internal parameters of the solar cell more difficult. This example shows the need for careful, accurate fitting to obtain reliable parameters.

## 6. Discussion

The FE model described here gives accurate, quantitative calculations of the electrical effects of the ITO layer on a solar cell. There are a number possible extensions that would be useful. This method could be used to optimize the conflicting requirements of low sheet resistance and high optical transmission. For instance, the calculation of the current generated by the active layer could include optical properties such as absorption and interference in the complete solar cell structure. Using this current as the boundary condition in the FE model, the effects of changing the ITO thickness could be calculated. An optimum design may have an ITO layer with varying thickness; thicker near the contact to accommodate the higher current and thinner far from the contact to be more transparent and allow a higher generated current.

One could also use the FE method to model metal contacts on the surface of the ITO, as would be the case with a commercial device. A section of the ITO surface opposite the active layer could be set as the $V = 0$ contact, rather than the edge of the ITO layer as in Fig. 2. The shadowing of the active layer would be including in the current boundary condition. A contact resistance could also be included by adding a thin resistive layer, which would also model the effects of current crowding at the contact.

In order to model a two dimensional contact grid pattern on the surface of a solar cell, Malm[30] used a three dimensional FE model. As we have shown, the current in the ITO layer is essentially only in the $x$-direction and is uniform across the thickness. With these assumptions, one can eliminate this dimension from the FE model and solve a two dimensional current flow problem for a sheet with the current generated by the active layer represented mathematically by a current source term over the area of the solar cell.

## 7. Conclusion

The FE model shows that the voltage drop in the ITO layer grows approximately as $L^2$. This voltage drop leads to a reduction of the net generated current of the solar cell in regions further away from the contact. The power loss is not only due to $I^2R$ losses, as is sometimes assumed in the literature, but also due to reduced current generated in the active layer. It was also found that the resulting power loss, due to the distributed resistance, is larger that the power loss from an equivalent lumped element resistance.

By fitting to data generated by the FE model, we have shown that the suns-$V_{oc}$ method gives the most reliable measure of $R_s$, compared to other commonly used methods. In particular, simply measuring the slope of the $IV$ curve at at large $V$ will not give a correct value for $R_s$. An accurate determination of model parameters of the active layer cannot be made without including the effects of the distributed resistance.

By fitting a diode model and the FE model to experimental data, we show that very small changes in the goodness of the fit can lead to significant differences the fit parameters. If one is attempting to analyze the mechanisms in the active layer with respect to some physical model, it is necessary to perform the fitting very carefully, including the distributed resistance in order to obtain accurate results.

## A. Appendix

Eq. 8 can be expressed in terms of the Lambert $W$ function which is defined by

$$X = Ye^{Y}, \quad \text{with solution } Y = W(X), \qquad (11)$$

where $W$ is the Lambert $W$ function.

Eq. 8 can be re-arranged as

$$\left(I + \frac{R_s}{R_{sh}}I - \frac{V}{R_{sh}} + I_L + I_0\right)\exp\left[\frac{q}{nkT}IR_s\right]$$
$$= I_0 \exp\left[\frac{q}{nkT}V\right]. \qquad (12)$$

Then, neglecting the term $\frac{R_s}{R_{sh}}I$ (since $R_s \ll R_{sh}$ and $I \ll 1$),

$$\frac{qR_s}{nkT}I_0 \exp\left(\frac{q}{nkT}\left[V - \frac{VR_s}{R_{sh}} + I_L R_s + I_0 R_s\right]\right)$$
$$= \frac{q}{nkT}\left[IR_s - \frac{VR_s}{R_{sh}} + I_L R_s + I_0 R_s\right] \qquad (13)$$
$$\times \exp\left(\frac{q}{nkT}\left[IR_s - \frac{VR_s}{R_{sh}} + I_L R_s + I_0 R_s\right]\right).$$

From this we can identify $Y$ and $X$. The solution, $Y = W(X)$, is written

$$\frac{q}{nkT}\left(IR_s - \frac{VR_s}{R_{sh}} + I_L R_s + I_0 R_s\right)$$
$$= W\left(\frac{qR_s}{nkT}I_0 \exp\left[\frac{q}{nkT}\left(V - \frac{VR_S}{R_{sh}} + I_L R_s + I_0 R_s\right)\right]\right). \qquad (14)$$

This can be solved for $I$ and gives Eq. 8.

## References

[1] D. Ginley, M. A. Green and R. Collins, "Solar Energy Conversion Toward 1 Terawatt," *MRS Bulletin* **33** (2008), 355-372.

[2] B. C. Thompson and J. M. J. Fréchet, "Polymer-Fullerene Composite Solar Cells," *Angew. Chem. Int. Ed.* **47** (2008), 58-77.

[3] C. W. Tang, "Two-layer organic photovoltaic cell," *Appl. Phys. Lett.* **48** (1986, 183-185.

[4] G. Yu, J, Gao, J. C. Humelen, F. Wudl and A. J. Heeger, "Polymer Photovoltaic Cells: Enhanced Efficiencies via a Network of Internal Donor-Acceptor Heterojunctions," *Science* **270** (1995), 1789-1791.

[5] S. Günes, H. Neugebauer, and N. S. Sariciftci, "Conjugated Polymer-Based Organic Solar Cells," *Chem. Rev.* **107** (2007), 1324-1338.

[6] A. C. Mayer, S. R. Scully, B. E. Hardin, M. W. Rowell, and M. D. McGehee, "Polymer-based solar cells", *Materials Today* **10**(11) (2007), 28-33.

[7] B. P. Rand, J. Genoe, and J Poortmans, "Solar Cells Utilizing Small Molecular Weight Organic Semiconductors", *Prog. Photovolt: Res. Appl.* **15** (2007), 659-676.

[8] M. T. Lloyd, J. E. Anthony, and G. G. Malliaras, "Photovoltaics from soluble small molecules", *Materials Today* **10**(11) (2007), 34-41.

[9] E. Bundgaard and F. C. Krebs, "Low band gap polymers for organic photovoltaics", *Sol. Energy Mater. Sol. Cells* **91** (2007), 954-985.

[10] J. Bouclé, P. Ravirajan, and J. Nelsen, "Hybrid polymer-metal oxide thin films for photovoltaic applications", *J. Mater. Chem.* **17** (2007), 3141-3153.

[11] M. Jøgensen, K. Norman, and F. C. Krebs, "Stability/degradation of polymer and organic solar cells", *Sol. Energy Mater. Sol. Cells* **92** (2008), 686-714.

[12] B. Zimmermann, M. Glatthaar, M. Niggemann, M. K. Riede, A. Hinsch, and A. Gombert, "ITO-free wrap through organic solar cells - A module concept for cost-efficient reel-to-reel production", *Sol. Energy Mater. Sol. Cells* **91** (2007), 374-378.

[13] M. Strange, D. Plackett, M. Kaasgard, and F. C. Krebs, "Biodegradable polymer solar cells", *Sol. Energy Mater. Sol. Cells* **92** (2008), 805-813.

[14] B. Winther-Jensen and F. C. Krebs, "High-conductivity large-area semitransparent electrodes for polymer photovoltaics by silk screen printing and vapour-phase deposition", *Sol. Energy Mater. Sol. Cells* **90** (2006), 123-132.

[15] W. Ma, C. Yang, X. Gong, K. Lee and A. J. Heeger, "Thermally Stable, Efficient Polymer Solar Cell with Nanoscale Control of the Interpenetrating Network Morphology," *Adv. Funct. Mater.* **15** (2005), 1617-1662.

[16] G. Li, V. Shrotriya, J. Huang, Y. Yao, T. Moriaty, K. Emery and Y. Yang, "High-efficiency solution processable polymer photovoltaic cells by self-organization of polymer blends," *Nature Materials* **4** (2005), 864-868.

[17] J. Y. Kim, K. Lee, N. E. CD. Moses, T.-Q. Nguyen, M. Dante and A. J. Heeger, "Efficient Tandem Polymer Solar Cells Fabricated by All-Solution Processing," *Science* **317** (2007), 222-225.

[18] M.-S. Kim, M.-G. Kang, L. J. Guo and J. Kim, "Choice of electrode geometry for accurate measurement of organic photovoltaic cell performance," *Appl. Phys. Lett.* **92** (2008), 133301.

[19] W.-J. Yoon and P. R. Berger, "4.8% efficient poly(3-hexylthiophene)-fullerene derivative (1:0.8) bulk heterojunction photovoltaic devices with plasma treated AgO$_x$/indium tin oxide anode modification," *Appl. Phys. Lett.* **92** (2008), 013306.

[20] A. Cravino, P. Schilinsky and C. J. Brabec, "Characterization of Organic Solar Cells: the Importance of Device Layout," *Adv. Funct. Mater.* **17** (2007), 3906-3910.

[21] M. D. Irwin, D. B. Buchholz, A. W. Hains, R. P. H. Chang and T. J. Marks, "p-Type semiconducting nickel oxide as an efficiency-enhancing anode interfacial layer in polymer bulk-heterojunction solar cells," *PNAS* **105** (2008), 2783-2787.

[22] J.-Y. Lee, S. T. Connor, Y. Cui, and P. Peumans, "Solution-Processed Mesh Transparent Electrodes", *Nano Letters* **8** (2008), 689-692.

[23] A. Gadisa, K. Tvingstedt, S. Admassie, L. Lindell, X. Crispin, M. R. Anderson, W. R. Salaneck, and O. Inganäs, "Transparent polymer cathode for organic photovoltaic devices", *Synthetic Metals* **156** (2006), 1102-1107.

[24] T. Aernouts, P. Vanlaeke, W. Geens, J. Poortmans, P. Heremans, S. Borghs, R. Mertens, R. Andriessen, and L. Leenders, "Printable anodes for flexible organic solar cell modules", *Thin Solid Films* **451-452** (2004), 22-25.

[25] K. Tvingstedt and O. Inganäs, "Electrode Grids for ITO-free Organic Photovoltaic Devices", *Adv. Mater.* **19** (2007), 2893-2897.

[26] (M. Wolf and H. Rauschenbach, "Series resistance Effects on Solar Cell Measurements", *Advanced Energy Conversion* **3** (1963), 455-479.

[27] R. J. Handy "Theoretical Analysis of the Series Resistance of a Solar Cell," *Solid-State Electronics* **10** (1967), 765-775.

[28] L. D. Nielson, "Distributed Series Resistance Effects in Solar Cells," *IEEE Trans. Electron Dev.* **ED-29** (1982), 821-827.

[29] P. Schilinsky, C. Waldauf, J. Hauch, and C. J. Brabec, "Simulation of light intensity dependent current characteristics of polymer solar cells", *J. Appl. Phys.* **95** (2004), 2816-2819.

[30] U. Malm and M. Edoff, "Influence From Front Contact Sheet Resistance on Extracted Diode Parameters in CIGS Solar Cells," *Progress in Photovoltaics: Research and Applications* **16** (2007), 113-121.

[31] A. K. Pandey, J. M. Nunzi, B. Ratier, and A. Moliton, "Size effect on organic optoelectronics devices: Example of photovoltaic cell efficiency," *Phys. Lett. A*, **372** (2008), 1333-1336.

[32] C. Lungenschmied, G. Dennler, H. Neugebauer, S. N. Sariciftci, M. Glatthaar, T. Meyer, and A. Meyer, "Flexible, long-lived, large-area, organic solar cells," *Sol. Energy Mater. Sol. Cells* **91** (2007), 379-384.

[33] D. Pysch, A. Mette, and S. W. Glunz, "A review and comparison of different methods to determine the series resistance of solar cells," *Solar Energy Materials and Solar Cells* **91** (2007), 1698-1706.

[34] M. Sabry and A. E. Ghitas, "Influence of Temperature on Methods for Determining Silicon Solar Cell Series Resistance," *J. Solar Energy Eng.* **129** (2007), 331-335.

[35] J. N. Reddy, *An Introduction to the Finite Element Method*, 2nd Ed., McGraw-Hill, Inc., USA, 1993, 297-301.

[36] K. K. Govil, "Maximum-power points of solar cells with simultaneous series and shunt resistances," *Int. J. Electronics* **56** (1984), 223-227.

[37] P. Hruska, Z. Chobola, and L. Grmela, "Diode I-U Curve Fitting with Lambert W Function," *Proc. 25th International Conference on Microelectronics (MIEL 2006)*, Belgrade, Serbia and Montenegro, 14-17 May, 2006, 468-471.

[38] R. M. Corless, G. H. Gonnet, D. E. G. Hare, D. J. Jeffrey, and D. E. Knuth, "On the Lambert W function," *Advances in Computational Mathematics* **5** (1996), 329-259.